Biosensors and Bioelectronics 36 (2012) 179–185

Contents lists available at SciVerse ScienceDirect

Biosensors and Bioelectronics

journal homepage: www.elsevier.com/locate/bios

Reduced graphene oxide/PAMAM–silver nanoparticles nanocomposite modified electrode for direct electrochemistry of glucose oxidase and glucose sensing

Zhimin Luo [a], Lihui Yuwen [c], Yujie Han [a], Jing Tian [a], Xingrong Zhu [a], Lixing Weng [b,*], Lianhui Wang [a,c,**]

[a] Laboratory of Advanced Materials, Fudan University, 220 Handan Road, Shanghai 200433, PR China
[b] College of Geography and Biological Information, Nanjing University of Posts and Telecommunications, 9 Wenyuan Road, Nanjing 210046, PR China
[c] Jiangsu Key Laboratory for Organic Electronics & Information Displays and Institute of Advanced Materials (IAM), Nanjing University of Posts and Telecommunications, 9 Wenyuan Road, Nanjing 210046, PR China

ARTICLE INFO

Article history:
Received 31 January 2012
Received in revised form
26 March 2012
Accepted 9 April 2012
Available online 20 April 2012

Keywords:
Graphene
Silver nanoparticles
Nanocomposite
Direct electrochemistry
Biosensor

ABSTRACT

Reduced graphene oxide/PAMAM–silver nanoparticles nanocomposite (RGO–PAMAM–Ag) was synthesized by self-assembly of carboxyl-terminated PAMAM dendrimer (PAMAM-G3.5) on graphene oxide (GO) as growing template, and in-situ reduction of both $AgNO_3$ and GO under microwave irradiation. The RGO–PAMAM–Ag nanocomposite was used as a novel immobilization matrix for glucose oxidase (GOD) and exhibited excellent direct electron transfer properties for GOD with the rate constant (K_s) of 8.59 s^{-1}. The fabricated glucose biosensor based on GOD electrode modified with RGO–PAMAM–Ag nanocomposite displayed satisfactory analytical performance including high sensitivity (75.72 μA mM^{-1} cm^{-2}), low detection limit (4.5 μM), an acceptable linear range from 0.032 mM to 1.89 mM, and also preventing the interference of some interfering species usually coexisting with glucose in human blood at the work potential of −0.25 V. These results indicated that RGO–PAMAM–Ag nanocomposite is a promising candidate material for high-performance glucose biosensors.

1. Introduction

Electron transfer in biological systems is a very important phenomenon in the areas of biochemical and biophysical sciences. The direct electron transfer (DET) reactions between redox proteins and electrode surface have attracted considerable interest, because studies of DET are useful for elucidating the relationship between the structure and biological functions of redox proteins (Gooding et al., 2003; Nassar et al., 1996; Pulcu et al., 2007; Reed and Hawkridge, 1987; Rusling and Nassar, 1993; Wang et al., 2002), and especially meaningful for development of biosensor (Liu et al., 2005) and biofuel cell (Tanne et al., 2010; Tasca et al., 2008). Glucose oxidase (GOD), a flavin enzyme with molecular weight of 150–180 kDa, has been extensively used to monitor the blood glucose levels in diabetics for its catalytic ability to glucose. However, the realizing of DET between GOD and the electrode is extremely difficult due to the active site of GOD, flavin adenine dinucleotide (FAD), being deeply embedded within a protective protein shell (Liu et al., 2005). In order to promote the direct electron transfer between active site of GOD and electrode, many materials, including molecular wire (Liu et al., 2007a), polymers (Liu et al., 2007a; Wang and Chen, 2009; Wang et al., 2009; Zhao et al., 2009), metal or metal oxide nanoparticles (Gao and Zheng, 2009; Salimi et al., 2007; Zhao et al., 2006), carbon nanotube (Tominaga et al., 2008; Vaze et al., 2009; Zhao et al., 2010), have been used to modify the electrode to immobilize GOD for improving the DET of GOD on the surface of electrode.

Graphene, a monolayer of sp^2 hybridized carbon atoms packed into a dense honeycomb crystal structure (Allen et al., 2009), has received increasing attention during recent years because of its unique physicochemical properties including high surface area (Li et al., 2008), excellent electric conductivity (Geim and Novoselov, 2007), strong mechanical strength, biocompatibility, ease of functionalization and mass production (Shao et al., 2009). It has shown great promise in applications as electrode materials for immobilizing GOD and improving DET of GOD on electrode (Kang et al., 2009; Liu et al., 2010; Shan et al., 2009; Wang et al., 2009c). Moreover, graphene-based hybrids have been proved to generate synergy effect and thus enhance their performance in applications of biosensor (Shan et al., 2010; Wu et al., 2009). For example, coupling graphene with CdS quantum dots resulted in facilitating direct electron transfer and retaining the good bioactivity of GOD via synergy effect (Wang et al., 2011). Silver nanoparticles (Ag NPs) have attracted our attention due to their quantum

* Corresponding author.
** Corresponding author.
E-mail addresses: lxweng@njupt.edu.cn (L. Weng), wlhui@fudan.edu.cn (L. Wang).

0956-5663/$ - see front matter © 2012 Elsevier B.V. All rights reserved.
http://dx.doi.org/10.1016/j.bios.2012.04.009

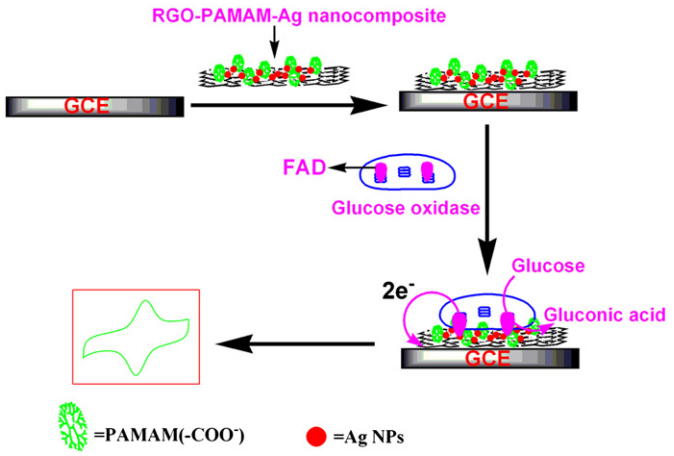

Fig. 1. Schematic diagram of RGO–PAMAM–Ag nanocomposite modified glassy carbon electrode to promote DET of GOD for detecting glucose.

characteristics and large specific surface area of small granule diameter as well as their ability to quickly transfer photoinduced electrons at the surfaces of colloidal particles (Liu et al., 2003). It has been reported that Ag NPs can greatly enhance the DET between some redox proteins and electrode (Gan et al., 2004; Liu and Hu, 2009; Ren et al., 2005).

Herein, RGO–PAMAM–Ag nanocomposite was synthesized by microwave-irradiation method and used to modify glassy carbon electrode (GCE). GOD was immobilized on the modified GCE and the DET between GOD and the modified GCE was studied, as can be illustrated in Fig. 1. The electrochemical catalytic activity of the fabricated electrode in response to glucose was also investigated. Due to the synergy effect of RGO and PAMAM–Ag NPs, the fabricated electrode showed excellent direct electrochemical behavior and the DET between the GOD and the modified electrode was easily achieved, indicating that RGO–PAMAM–Ag nanocomposite could be a good candidate material for immobilizing biomolecules and fabricating the third-generation biosensor.

2. Experimental section

2.1. Reagents and apparatus

Graphite, PAMAM dendrimer (ethylenediamine core, generation 3.5 solution in methanol), Chitosan (CS, medium molecular weight with viscosity 200–800 cP of 1% solution in 1% acetic acid, 75–85% deacetylated) and glucose oxidase (GOD, from *Aspergillus niger* Type X-S, lyophilized powder, 100,000–250,000 units/g solid) were purchased from Sigma-Aldrich. Acetone, potassium permanganate ($KMnO_4$, 99%), concentrated sulfuric acid (H_2SO_4, 98%), silver nitrate ($AgNO_3$, 99.9%) and hydrazine hydrate (50%) were purchased from Aladdin Reagent Co., Ltd. All reagents were of analytical grade and were used as received. Aqueous solutions were prepared with deionized water from a Millipore system.

The UV–vis absorption spectra were carried out with a UV–VIS–NIR spectrophotometer (Shimadzu **UV-3150**). Morphology and element analyses of RGO–PAMAM–Ag nanocomposite were carried out on high solution transmission electron microscopy (HRTEM) (JEOL, **JEM**-2010F **UHR**) equipped with an energy dispersive X-ray spectrometer (EDS), operating at 200 kV. The sample was prepared by dropping RGO–PAMAM–Ag nanocomposite on micro-grids supported on a 200 mesh copper grid and allowing deionized water to dry for observation. The electrochemical experiments were performed with a CHI660d electrochemical workstation (CHI, Austin, TX). All measurements were conducted at room temperature (25 °C) with a conventional three-electrode cell, which included a Ag/AgCl (saturated KCl solution) as reference electrode, a platinum wire as counter electrode, and a bare or modified GCE (3 mm in diameter) as working electrode. The cyclic voltammograms (CVs) experiments were carried out at a scan rate of 100 mV s^{-1} in a quiescent solution, which had been purged with high-purity nitrogen for at least 20 min prior to experiments. The chronoamperometric experiments were carried out in O_2-saturated phosphate buffered saline (PBS) with successive adding glucose solution at the work potential of −0.25 V.

2.2. Preparation of GO

Natural graphite was used for the preparation of GO. Graphite oxide was prepared from natural graphite powder by Hummers and Offeman's method with some modifications (Hummers and Offeman, 1958). In brief, 1 g of graphite powder and 30 mL of sulfuric acid were added into a reaction vessel in a dry ice bath, and stirred gently for 6 h. Then 3 g of potassium permanganate was added slowly with violent stirring. The reaction was allowed to proceed at below 20 °C for 30 min and at 35 °C for 30 min. Then 30 mL of deionized water was added into the reaction vessel slowly, and the reaction was kept at ~95 °C for 35 min. At last 140 mL of deionized water and 10 mL of 30% hydrogen peroxide were added into the reaction vessel for finishing the reaction. The resulting graphite oxide was filtered and washed with 5% hydrochloric acid and deionized water to remove the free SO_4^{2-}. The graphite oxide was suspended in the deionized water, and exfoliated through ultrasonication for 3 h. The colloidal solution was centrifuged at the speed of 5000 rpm for 10 min to remove the unexfoliated graphite oxide. The yellow-brown upper solution was used to prepare RGO–PAMAM–Ag nanocomposite.

2.3. Preparation of RGO–PAMAM–Ag nanocomposite

1 mL of GO (1 mg mL^{-1}) and 100 μL of PAMAM-G3.5 dendrimer methanol solution was added into a reaction vessel and diluted with 19.0 mL of deionized water. The mixture was stayed for 1 h in order to fully make PAMAM-G3.5 dendrimer self-assembled on GO. Then 260 μL of 0.2 M $AgNO_3$ aqueous solution was added and the mixtures were kept in the microwave reactor for 60 min under violent stirring at 80 °C. The resultant solution was firstly filtered by microporous membrane (pore size 0.22 μm) and rinsed with deionized water. The solid on the microporous membrane was dispersed in 20 mL deionized water, and the pH value of the colloidal solution was adjusted to be 10.0 with 1.0 M NaOH aqueous solution. Then 1.4 μL of hydrazine hydrate (50%) was added to further react for 2 h at 90 °C. The product was obtained through filtration by microporous membrane (pore size 0.22 μm) and rinsed with deionized water again. The RGO–PAMAM–Ag nanocomposite was redispersed in water (pH 10.0) and was used to modify the GCE.

2.4. Fabrication of modified electrode

GCE (3 mm diameter) was polished with 1.0, 0.3, and 0.05 μm α-alumina powders, respectively. After successive ultrasonication in ethanol and deionized water, the electrode was rinsed with deionized water and allowed to dry at room temperature. 6 μL of RGO–PAMAM–Ag suspension (=0.25 mg mL^{-1}) was dropped on the surface of GCE and dried in air. Then the modified electrode (GCE/RGO–PAMAM–Ag) was put into phosphate buffered saline (PBS) (pH 5.29) for 1 h to reduce the negative charges on the surface of RGO–PAMAM–Ag, and immersed into 10 mg mL^{-1} GOD solution in 0.1 M PBS (pH 7.0) for 24 h to load GOD. Finally, 10 μL

of CS solution (5 mg mL^{-1}, prepared by dissolving 50 mg CS in 10 mL 1% HAC solution) was dropped on the surface of GCE modified with RGO–PAMAM–Ag-GOD and dried at room temperature. The modified electrode (GCE/RGO–PAMAM–Ag/GOD/CS) was immersed in 0.1 M PBS (pH 7.0) to remove the loosely adsorbed GOD and stored at 4 °C in a refrigerator under dry conditions for further use.

3. Results and discussion

3.1. Preparation and characterization of RGO–PAMAM–Ag nanocomposite

RGO–PAMAM–Ag nanocomposite was synthesized by microwave-assisted hydrothermal method. The process of synthesizing RGO–PAMAM–Ag nanocomposite was illustrated in Fig. S1. Firstly, GO was synthesized through colloidal chemistry method. It is noted that GO contains a wide range of oxygen-containing functional groups including hydroxyl, epoxy, and carboxylic groups both on the basal planes and at the edges of graphene oxide sheets (Park et al., 2009). PAMAM-G3.5 dendrimer is a kind of amphiphilic macromolecules and contains imino and terminal carboxylic groups. PAMAM-G3.5 can self-assemble on GO quickly through hydrogen-bonding interactions between imino groups of PAMAM-G3.5 and the oxygen-containing functional groups of GO, and hydrophobic interactions between the alkyl groups of PAMAM-G3.5 and aryl groups of GO. After the self-assembly of PAMAM-G3.5, GO-PAMAM acts as templates. The carboxylic and imino groups on GO-PAMAM can combine Ag^+, then both GO and Ag^+ are reduced under microwave irradiation at 80 °C. The product is preliminary reduced graphene oxide/Ag NPs nanocomposite (PRGO–PAMAM–Ag). 50% hydrazine hydrate was added to further reduce GO. RGO does not aggregate together through π–π stacking because the existence of PAMAM on its surface. RGO–PAMAM–Ag nanocomposite is stable for at least two months in the aqueous solution (pH 10.0).

The role of PAMAM-G3.5 dendrimer as reductant in reducing $AgNO_3$ was proved by the phenomenon that there is no Ag NPs forming in the reaction only with GO and $AgNO_3$. UV–vis absorption spectrum was used to study the synthesis of RGO–PAMAM–Ag, as shown in Fig. 2A. The spectrum of GO dispersion in water presents two characteristic features, a peak at 228 nm, corresponding to the $\pi \rightarrow \pi^*$ transitions of aromatic C–C bonds, and a shoulder around 303 nm, assigned to $n \rightarrow \pi^*$ transitions of C=O bonds on basal plane of GO (Li et al., 2008). The absorption peak of GO at 228 nm redshifts to 253 nm in PRGO–PAMAM–Ag after microwave-assisted reaction for 60 min at 80 °C, and redshifts to 268 nm in RGO–PAMAM–Ag after being further reduced for 2 h by hydrazine hydrate, which indicates the restoration of the electronic conjugation within the graphene sheets (Li et al., 2008). The disappearance of absorption peak at 303 nm in PRGO–PAMAM–Ag and RGO–PAMAM–Ag indicates successfully removing the carbonyl group on GO through reduction (Villar-Rodil et al., 2009). The absorption at around 410 nm in PRGO–PAMAM–Ag and 422 nm in RGO–PAMAM–Ag clearly indicates the formation of Ag NPs, which arises due to the excitation of surface plasmon in the Ag NPs (Pasricha et al., 2009). The surface plasmon band of Ag NPs in the PRGO–PAMAM–Ag is located at 410 nm, which redshifts to 422 nm in RGO–PAMAM–Ag due to the change in the dielectric environment and the electron density of the Ag NPs induced by graphene sheets after further reduction with hydrazine hydrate (Li and Liu, 2010). Compared with absorption of Ag NPs synthesized on GO-PAMAM-G3.5 template, UV–vis absorption spectra of Ag NPs synthesized in the PAMAM-G3.5 solution under the same condition have a shoulder peak at 437 nm besides the absorption of 410 nm, which may be explained that PAMAM-G3.5 aggregates lead to form various shapes of Ag NPs such as torispherical and triangle in solution phase (Kavitha et al., 2009).

Graphene, has a unique two-dimensional structure and exhibits distinct electrical and spectroscopic properties, including strong and simple resonance Raman signatures. Raman spectroscopy has received considerable attention in research on the graphene or its nanocomposite, because it can reflect many properties of graphene and their interaction with other nanomaterials such as metal NPs (Au, Ag) (Yang et al., 2010). The characteristic Raman bands in GO or RGO are G band at 1580 cm^{-1} and D band at 1345 cm^{-1}. G band is usually assigned to the E_{2g} phonon of C sp^2 atoms, and D band is a breathing mode of κ-point phonons of A_{1g} symmetry (Zhou et al., 2009b). Several studies have shown that the Raman signals of GO or RGO deposited with Ag NPs can be enhanced, and in these instances GO or RGO acts as testing molecules to investigate the SERS effect (Pasricha et al., 2009; Xu and Wang, 2009; Zhou et al., 2009a). In this system, Raman spectroscopy is also used to study the interaction between GO or RGO and Ag NPs assembled on them. As shown in Fig. 2B, Raman intensity of D band (I_D) and G band (I_G) in RGO–PAMAM–Ag nanocomposite increased markedly in comparison with GO without Ag NPs, which may be explained by chemical mechanism related to charge transfer (CT) between RGO and Ag NPs (Li and Liu, 2010). The intensity ratio of D to G peak (I_D/I_G), known as Tuinstra–Koenig (TK) relation, is found to change inversely with graphitic domain size and widely used to study the crystalline quality of graphite or graphene after different kinds of treatment (Paredes et al., 2009). Compared with I_D/I_G ratio (1.44) of RGO prepared by hydrazine hydrate directly (Zhou et al., 2009b), the I_D/I_G ratio (1.08) of RGO–PAMAM–Ag was lower, which indicates that Ag NPs and PAMAM-G3.5 dendrimer assembled on RGO can decrease the defects of RGO to some extent in the process of reduction with hydrazine hydrate.

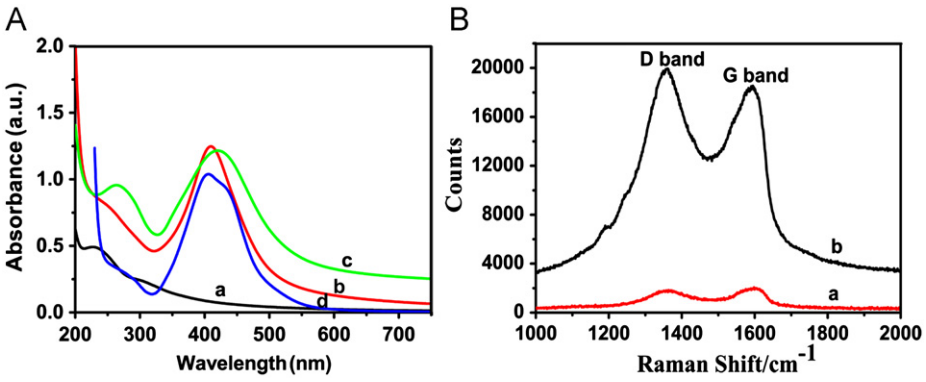

Fig. 2. (A) The UV–vis absorption spectra of GO (a), PRGO–PAMAM–Ag (b), RGO–PAMAM–Ag (c), PAMAM–Ag (d). (B) Raman spectra of GO (a) and RGO–PAMAM–Ag (b).

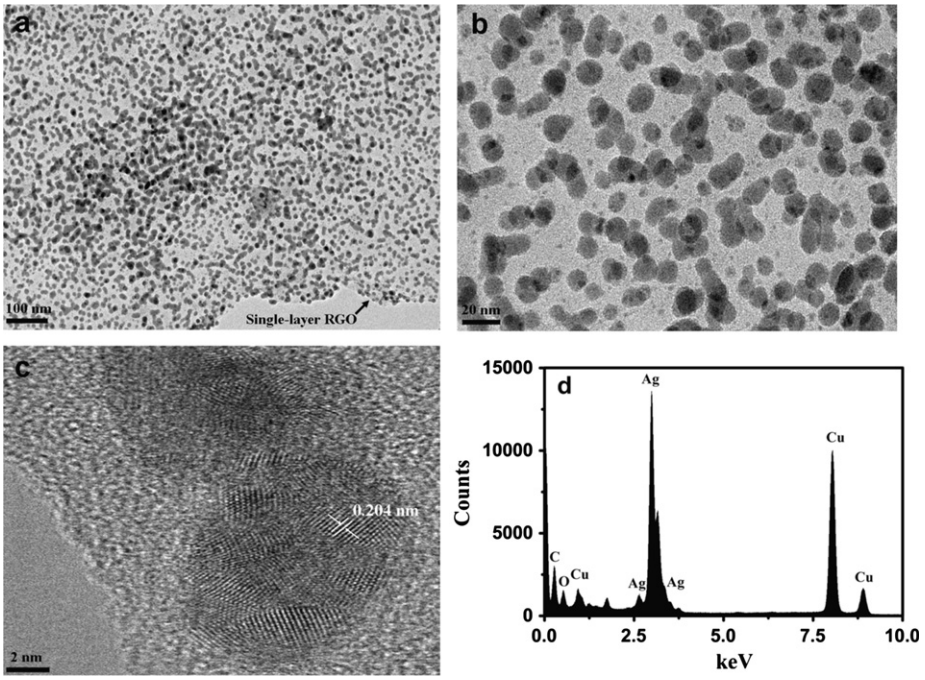

Fig. 3. TEM images of RGO–PAMAM–Ag on copper micro-grid (a, b), HRTEM image of Ag NPs assembled on RGO (c), and EDS analysis confirmation of Ag element (d).

The morphology of RGO–PAMAM–Ag nanocomposite was characterized by TEM and HRTEM. Fig. 3(a, b) shows TEM image of RGO–PAMAM–Ag nanocomposite, revealing that the RGO–PAMAM–Ag consisted of 2D RGO sheets decorated with many Ag NPs, and the individual torispherical Ag NPs with an average diameter of 12.5 nm are well separated from each other and homogeneously spread out on the RGO sheets. A single-entity Ag NPs embedded in the RGO was presented in Fig. 3c, where the crystal lattice of Ag NPs is distinct. The measured interplanar spacing for the lattice fringes is 0.204 nm, which corresponds to the {200} lattice plane of face-centered-cubic (fcc) silver, revealing that the growth plane of the Ag NPs is one of the {200} planes (Guo et al., 2008; Yu and Yam, 2005). The EDS analysis in Fig. 3d also confirmed that the surface of RGO sheets was covered by Ag NPs.

3.2. Electrochemical characterization of GCE/RGO–PAMAM–Ag/GOD/CS

RGO–PAMAM-G3.5–Ag nanocomposite was used for modifying GCE and then GOD was loaded on the modified electrode. The DET of GOD immobilized on the modified electrode was investigated in N_2-saturated PBS (0.1 M, pH 7.0) through CVs. As shown in Fig. 4, The formal potential of GCE/RGO–PAMAM–Ag/GOD/CS, calculated from the average value of the anodic and cathodic peak potentials, is about −0.381 V (vs. Ag/AgCl) and the CVs of GCE/RGO–PAMAM–Ag/GOD/CS shows a pair of well-defined and nearly reversible redox peaks at −0.362 V and −0.402 V with the peak-to-peak separation (ΔE_p) of 40 mV at 100 mV s^{-1} (curve c in Fig. 4). In contrast, no peak is observed at bare GCE (curve a in Fig. 4) and GCE/RGO–PAMAM–Ag (curve b in Fig. 4), which indicates they are electrochemically silent in this potential window. Furthermore, after incubation of GCE/RGO–PAMAM–Ag/GOD/CS and GCE/RGO–PAMAM–Ag/FAD/CS in 3 M guanidine hydrochloride solution for six days, the redox peaks of GCE/RGO–PAMAM–Ag/GOD/CS almost disappeared, while that of GCE/RGO–PAMAM–Ag/FAD/CS still remained at 34% of the initial one, which can be seen in Fig. S2. Because treatment of the GCE/RGO–PAMAM–Ag/GOD/CS with concentrated salt solution can easily strip the FAD active center from the GOD molecule or remove the adsorbed GOD from the electrode surface, and it is relatively

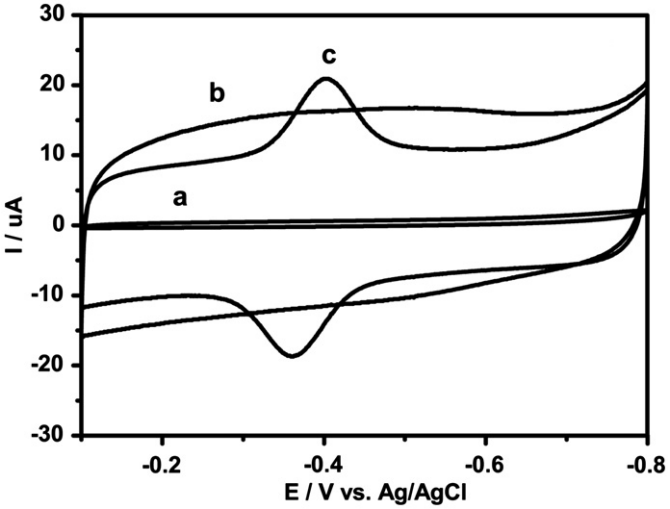

Fig. 4. CVs of GCE (a), GCE modified with RGO–PAMAM–Ag (b) and RGO–PAMAM–Ag–GOD–CS (c) in N_2-saturated PBS (0.1 M, pH 7.0) at a scan rate of 100 mV s^{-1}.

ineffective in removing adsorbed free FAD from the electrode surface (Cai and Chen, 2004; Ianniello et al., 1982), the experimental results suggest that the redox peaks at GCE/RGO–PAMAM–Ag/GOD/CS are attributed to the DET for the conversion of GOD (FAD) to GOD ($FADH_2$) and not to free FAD, which may have dissociated away from GOD due to conformational changes during immobilization. The smaller ΔE_p value indicated the faster DET between the redox active site of GOD (the cofactor FAD) and the modified GCE without the help of electron transfer mediator (Deng et al., 2009). It can be observed from Fig. S3 that there are no evident redox peaks attributed to the DET of GOD at RGO–PAMAM (curve A in Fig. S3), PAMAM (curve B in Fig. S3) and Ag–PAMAM (curve C in Fig. S3) modified GCE. Furthermore, the ΔE_p of GCE/RGO–PAMAM–Ag/GOD/CS (40 mV) is smaller than that of GCE/RGO/GOD/CS (46 mV), which indicating that RGO–PAMAM–Ag nanocomposite plays an important role in facilitating the DET (Liu et al., 2007b).

It is well known that the direct electrochemistry of GOD is a two-electron coupled with two-proton reaction and therefore, peak potentials should be pH-dependent (Wang et al., 2011). Fig. 5C shows CVs of the RGO–PAMAM–Ag modified electrode in 0.1 M PBS with different pH values. In each solution, a pair of stable and well-defined reversible redox peaks of the GOD was observed. Furthermore, negative shifts in both anodic and cathodic peak potentials are observed with increasing pH value from 6.0 to 8.0, which indicates that the hydrogen ion is involved in the electrode reaction of GOD. This result is in good agreement with previous reports (Deng et al., 2008; Liu et al., 2005; Wang et al., 2011). In addition, as shown in Fig. 5D, the formal potential has a linear relationship with pH from 5.0 to 8.0 with a slope of -50.8 ± 2.05 mV/pH, which is close to the theoretical value of -58.6 mV/pH for a reversible reaction coupled with two-proton and two-electron transfer electrochemical process (Liu et al., 2005). All of these indicate that two protons ($2H^+$) and two electrons ($2e^-$) maybe participate in the direct electrochemical reaction of GOD immobilized on the modified electrode.

Based on these results, the effect of scan rates on the CVs responses of immobilized GOD has also been investigated. As shown in Fig. 5A, with the scan rate increasing, the cathodic and anodic peak currents increased simultaneously in N_2-saturated PBS (0.1 M, pH 7.0). The peak separation (ΔE_p) ranged from 44 mV to 148 mV with the scan rate increasing from 0.05 V s^{-1} to 2.0 V s^{-1}, possibly because of the resistance of the modified layer (Bao et al., 2008). Because $n\Delta E_p$ is greater or equal to 200 mV, the DET constant (K_s) of the GOD in the modified electrode can be estimated by using the Laviron's model (Laviron, 1979). Plots of the E_{pa} and E_{pc} vs. the logarithm of the scan rates produce two straight lines with slops of $2.3RT/(1-\alpha)nF$ and $-2.3RT/\alpha nF$ at high scan rates (Fig. 5B) (Zhao et al., 2008). From the slopes, α is estimated to be 0.44. The K_s of the GOD immobilized on the modified electrode was calculated to be about 8.59 s^{-1} according to the equation of

$$\mathrm{Log}K_s = \alpha\mathrm{Log}(1-\alpha)+(1-\alpha)\mathrm{Log}\alpha-\mathrm{Log}\frac{RT}{nF\nu}-\frac{\alpha(1-\alpha)nF\Delta E_p}{2.3RT}.$$

This K_s is higher than those reported previously on graphene-CS (2.83 s^{-1}) (Kang et al., 2009), on graphene-CdS (5.9 s^{-1}) (Wang et al., 2011), on SWCNTs-CS (3.0 s^{-1}) (Zhou et al., 2008), on CNTs-poly (diallyldimethylammonium chloride) (PDDA) (2.76 s^{-1}) (Wen et al., 2007), and on MWCNTs-CS (7.73 s^{-1}) (Liu et al., 2005) modified electrode. These results suggest that the GCE modified with RGO–PAMAM–Ag nanocomposite provides fast DET between the redox center of GOD and the surface of electrode.

3.3. Study of electrocatalytic activity of GOD immobilized on modified electrode

In order to show the enzymatic activity of GOD immobilized on the modified electrode, further electrocatalytic experiments about the reaction between GOD and glucose were carried out. Fig. 6A shows the CVs of the modified electrode in N_2-saturated PBS (0.1 M, pH 7.0) and in O_2-saturated PBS (0.1 M, pH 7.0) without and with glucose at a scan rate of 100 mV s^{-1}. An increase in cathodic peak current and decrease in anodic peak current were observed in the O_2-saturated PBS in the absence of glucose as compared to the corresponding peaks in the N_2-saturated PBS, which is because of the electrochemically formed GOD ($FADH_2$) with electrocatalyzed reduction of O_2. Moreover, with addition of glucose to O_2-saturated PBS, the reduction current decreased. The higher glucose concentration was, the more reduction current decreased. It can be attributed to the fact that adding glucose

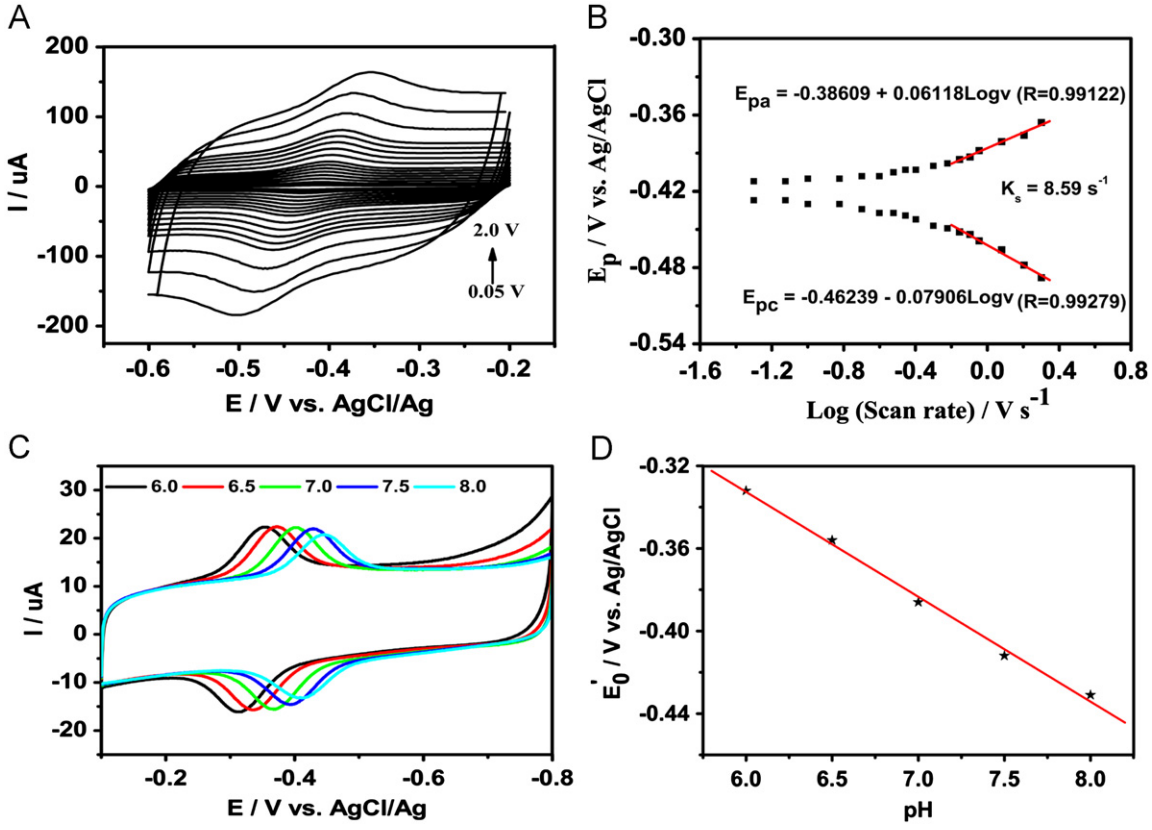

Fig. 5. (A) CVs of GCE/RGO–PAMAM–Ag/GOD/CS in N_2-saturated PBS (0.1 M, pH 7.0) at different scan rates from 0.05 V to 2.0 V. (B) The relationship of the peak potential (E_p) vs. the logarithm of scan rate (log v). (C) CVs of GCE/RGO–PAMAM–Ag/GOD/CS in N_2-saturated PBS (0.1 M, pH 7.0) with different pH values of 6.0, 6.5, 7.0, 7.5, and 8.0 at a scan rate of 100 mV s^{-1}. (D) The plot of formal potentials vs. pH.

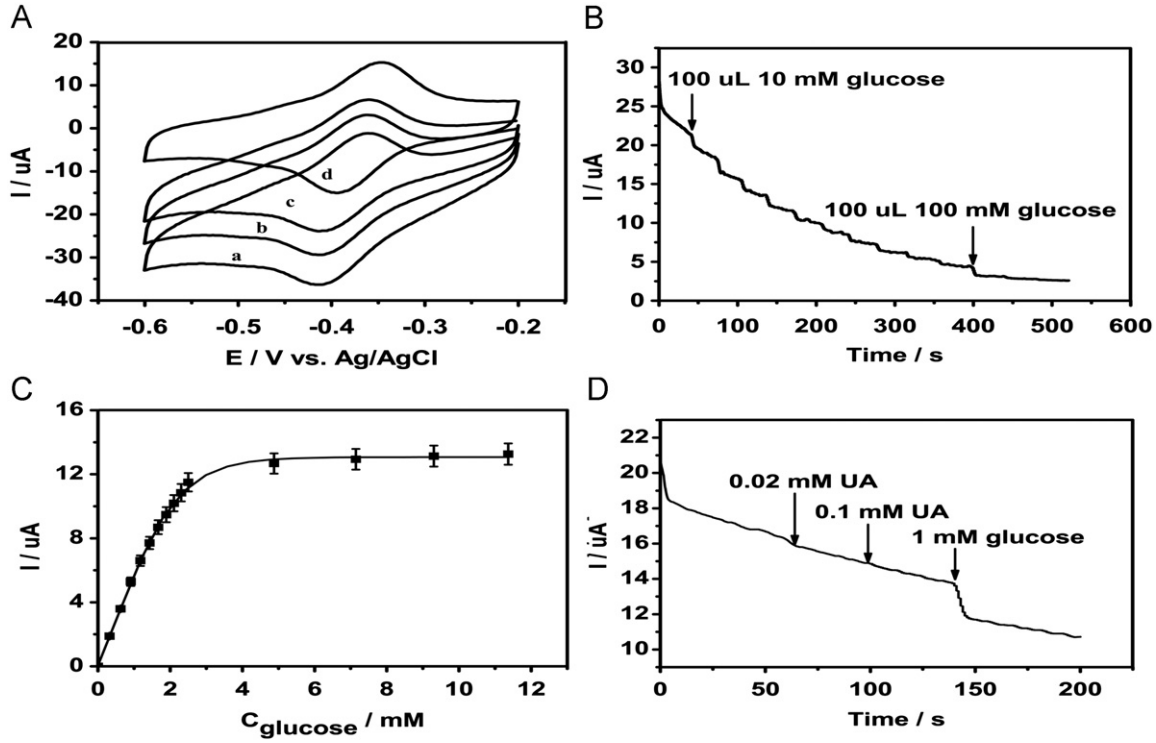

Fig. 6. (A) CVs of GCE/RGO–PAMAM–Ag/GOD/CS in O_2-saturated PBS (0.1 M, pH 7.0) in the absence of glucose (a), in the presence of 1.96 mM (b) and 3.85 mM (c) glucose, and in N_2-saturated PBS (0.1 M, pH 7.0) (d) at a scan rate of 100 mV s^{-1}. (B) Current–time response of GCE modified with RGO–PAMAM–Ag/GOD/CS with successive addition of 100 μL 10 mM glucose and 100 mM glucose into 3 mL O_2-saturated PBS (0.1 M, pH 7.0) at −0.25 V. (C) Calibration curve for glucose sensing corresponding to (B). (D) Current–time response of GCE/RGO–PAMAM–Ag/GOD/CS to 0.02 mM UA, 0.1 mM AA and 1.0 mM glucose at the work potential of −0.25 V in O_2-saturated PBS (0.1 M, pH 7.0).

promotes the enzyme-catalysis reaction of GOD and glucose, reduces the oxidized form of GOD on the modified electrode, and thus decreases the electrode reduction current (Wang et al., 2011, 2009c).

Under an applied potential of −0.25 V, amperometric determination of glucose was carried out. Fig. 6B shows the amperometric response of RGO–PAMAM–Ag modified enzyme electrode to successive addition of glucose. It was found that during successive addition of 100 μL 10 mM glucose and 100 mM glucose into 3 mL O_2-saturated PBS (0.1 M, pH 7.0) at –0.25 V, an evident current response is observed. The biosensor based on RGO–PAMAM–Ag modified enzyme electrode shows a fast response time of less than 10 s and exhibits an excellent linear response to glucose in the concentration range of 0.032–1.89 mM (R=0.996) (in Fig. 6C) with a detection limit of 4.5 μM (S/N=3). Furthermore, the sensitivity of the as-prepared biosensor was calculated to be 75.72 μA mM^{-1} cm^{-2}, which is higher than that of the glucose biosensors based on Au/PPF–CNTs–GOD (42 μA mM^{-1} cm^{-2}) (Muguruma et al., 2008), GCE/graphene–CS–GOD (37.93 μA mM^{-1} cm^{-2}) (Kang et al., 2009), GCE/CNTs–CdTe–Nafion–GOD (14.41 μA mM^{-1} cm^{-2}) (Liu et al., 2007b), GCE/CNTs–CS–GOD (7.36 μA mM^{-1} cm^{-2}) (Liu et al., 2005), and GCE/graphene–CdS–Nafion–GOD (1.76 μA mM^{-1} cm^{-2}) (Wang et al., 2011). The apparent Michealis–Menten constant (K_m) was also estimated to be 9.64 mM by using the Lineweaver–Burk equation (Kang et al., 2009). The result is comparable to those obtained from MWCNTs–CS–GOD (8.2 mM) (Liu et al., 2005) and Nafion–GOD–SWCNTs (8.5 mM) (Liu et al., 2008) modified electrodes, and is lower than PMMA–MWCNT(PDDA)/GOD–NFE (10.12 mM) (Manesh et al., 2008), GOD/Au_{nano}/Pt_{nano}/CNT/gold electrode(10.73 mM) (Chu et al., 2007), GOD–CS–SiO_2/Pt/MWNTs (14.4 mM) (Zou et al., 2008), GOD/prussian blue/MWCNT (18 mM) (Zhu et al., 2006), GOD/gold–MWCNT/Teflon (14.9 mM) and MWCNT/Teflon (30 mM) (Manso et al., 2007), indicating that the GCE modified with RGO–PAMAM–Ag–GOD–CS exhibits good affinity to glucose.

3.4. Interference

It is well known that there are some easily oxidative species such as dopamine, ascorbic acid (AA), uric acid (UA), and other carbohydrate compounds usually coexisting with glucose in human blood, which can be easily oxidized at the positive potential. The lower working potential may avoid the interference of dopamine, AA, UA and other carbohydrate compounds in the procedure of detecting glucose. The normal physiological level of glucose is 3–8 mM, which is much higher than those of interfering species of AA (~0.1 mM), UA (~0.02 mM), etc. (Meng et al., 2009). Since the interfering species have higher electron transfer rates than glucose, their oxidation currents are comparable to that of high concentrated glucose. Because a high real surface area of an electrode favors a kinetically controlled sluggish reaction (the electrooxidation for glucose), while the electrooxidation of the interfering species being diffusion-controlled does not depend significantly on the electrode surface (Yuan et al., 2005), it is expected that the enzyme electrode modified with RGO–PAMAM–Ag nanocomposite would give high sensitivity and selectivity for glucose detection under physiological conditions. The amperometric responses of the GCE/RGO–PAMAM–Ag/GOD/CS to the continuous addition of 0.02 mM UA, 0.1 mM AA, and 1.0 mM glucose at the applied potentials of −0.25 V in PBS (0.1 M, pH 7.0) were evaluated respectively. As can be seen in Fig. 6D, the interference from UA, AA is negligible at the working potential of −0.25 V. The reproducibility of this glucose biosensor was also identified by detecting 0.5 mM of glucose successfully for six times. The intraelectrode and interelectrode relative standard deviation (RSD) was found

to be 4.47% and 5.60%, which illustrates that the prepared electrode has an acceptable reproducibility.

4. Conclusions

In this study, RGO–PAMAM–Ag nanocomposite was prepared under microwave irradiation by using GO self-assembled with PAMAM-G3.5 dendrimer as growth templates. RGO–PAMAM–Ag nanocomposite can provide a unique microenvironment for the direct electrochemistry of GOD immobilized on the surface of modified electrode, which can keep its high electrocatalytic activities. A glucose biosensor based on RGO–PAMAM–Ag nanocomposite has been developed and displays satisfactory analytical performance with a wide linear range from 0.032 to 1.89 mM, high sensitivity ($75.72\ \mu A\ mM^{-1}\ cm^{-2}$), and low detection limit (4.5 μM) at the applied potential of −0.25 V. Interference from UA and AA that usually coexisting with glucose in blood samples is nearly negligible to this glucose biosensor. All these characteristics suggest that RGO–PAMAM–Ag nanocomposite is a novel kind of excellent material for fabricating glucose biosensors based on direct electron transfer.

Acknowledgments

This work was financially supported by the National Basic Research Program of China (973 Program, 2012CB933301, 2009CB930601), National Natural Science Foundation of China (90813010), and Ministry of Education of China (IRT1148).

Appendix A. Supporting information

Supplementary data associated with this article can be found in the online version at http://dx.doi.org/10.1016/j.bios.2012.04.009.

References

Allen, M.J., Tung, V.C., Kaner, R.B., 2009. Chemical Reviews 110, 132–145.
Bao, S.J., Li, C.M., Zang, J.F., Cui, X.Q., Qiao, Y., Guo, J., 2008. Advanced Functional Materials 18, 591–599.
Cai, C., Chen, J., 2004. Analytical Biochemistry 325, 285–292.
Chu, X., Duan, D., Shen, G., Yu, R., 2007. Talanta 71, 2040–2047.
Deng, C., Chen, J., Chen, X., Xiao, C., Nie, L., Yao, S., 2008. Biosensors & Bioelectronics 23, 1272–1277.
Deng, S., Jian, G., Lei, J., Hu, Z., Ju, H., 2009. Biosensors & Bioelectronics 25, 373–377.
Gan, X., Liu, T., Zhong, J., Liu, X., Li, G., 2004. ChemBioChem 5, 1686–1691.
Gao, R., Zheng, J., 2009. Electrochemistry Communications 11, 608–611.
Geim, A.K., Novoselov, K.S., 2007. Nature Materials 6, 183–191.
Gooding, J.J., Wibowo, R., Liu, J., Yang, W., Losic, D., Orbons, S., Mearns, F.J., Shapter, J.G., Hibbert, D.B., 2003. Journal of the American Chemical Society 125, 9006–9007.
Guo, S., Dong, S., Wang, E., 2008. Crystal Growth & Design 9, 372–377.
Hummers Jr, W.S., Offeman, R.E., 1958. Journal of the American Chemical Society 80. 1339–1339..
Ianniello, R.M., Lindsay, T.J., Yacynych, A.M., 1982. Analytical Chemistry 54, 1098–1101.
Kang, X., Wang, J., Wu, H., Aksay, I.A., Liu, J., Lin, Y., 2009. Biosensors & Bioelectronics 25, 901–905.
Kavitha, M., Parida, M.R., Prasad, E., Vijayan, C., Deshmukh, P., 2009. Macromolecular Chemistry and Physics 210, 1310–1318.
Laviron, E., 1979. Journal of Electroanalytical Chemistry and Interfacial Electrochemistry 101, 19–28.
Li, D., Muller, M.B., Gilje, S., Kaner, R.B., Wallace, G.G., 2008. Nature Nanotechnology 3, 101–105.
Li, J., Liu, C., 2010. European Journal of Inorganic Chemistry 2010, 1244–1248.
Liu, C.Y., Hu, J.M., 2009. Biosensors & Bioelectronics 24, 2149–2154.
Liu, G., Paddon-Row, M.N., Justin Gooding, J., 2007a. Electrochemistry Communications 9, 2218–2223.
Liu, Q., Lu, X., Li, J., Yao, X., 2007b. Biosensors & Bioelectronics 22, 3203–3209.
Liu, T., Zhong, J., Gan, X., Fan, C., Li, G., Matsuda, N., 2003. ChemPhysChem 4, 1364–1366.
Liu, X., Shi, L., Niu, W., Li, H., Xu, G., 2008. Biosensors & Bioelectronics 23, 1887–1890.
Liu, Y., Wang, M., Zhao, F., Xu, Z., Dong, S., 2005. Biosensors & Bioelectronics 21, 984–988.
Liu, Y., Yu, D., Zeng, C., Miao, Z., Dai, L., 2010. Langmuir 26, 6158–6160.
Manesh, K., Kim, H.T., Santhosh, P., Gopalan, A., Lee, K.P., 2008. Biosensors & Bioelectronics 23, 771–779.
Manso, J., Mena, M., Yanez-Sedeno, P., Pingarron, J., 2007. Journal of Electroanalytical Chemistry 603, 1–7.
Meng, L., Jin, J., Yang, G., Lu, T., Zhang, H., Cai, C., 2009. Analytical Chemistry 81, 7271–7280.
Muguruma, H., Shibayama, Y., Matsui, Y., 2008. Biosensors & Bioelectronics 23, 827–832.
Nassar, A.E.F., Rusling, J.F., Nakashima, N., 1996. Journal of the American Chemical Society 118, 3043–3044.
Paredes, J., Villar-Rodil, S., Solis-Fernandez, P., Martinez-Alonso, A., Tascon, J., 2009. Langmuir 25, 5957–5968.
Park, S., Dikin, D.A., Nguyen, S.B.T., Ruoff, R.S., 2009. Journal of Physical Chemistry C 113, 15801–15804.
Pasricha, R., Gupta, S., Srivastava, A.K., 2009. Small 5, 2253–2259.
Pulcu, G.S., Elmore, B.L., Arciero, D.M., Hooper, A.B., Elliott, S.J., 2007. Journal of the American Chemical Society 129, 1838–1839.
Reed, D.E., Hawkridge, F.M., 1987. Analytical Chemistry 59, 2334–2339.
Ren, X., Meng, X., Chen, D., Tang, F., Jiao, J., 2005. Biosensors & Bioelectronics 21, 433–437.
Rusling, J.F., Nassar, A.E.F., 1993. Journal of the American Chemical Society 115, 11891–11897.
Salimi, A., Sharifi, E., Noorbakhsh, A., Soltanian, S., 2007. Biosensors & Bioelectronics 22, 3146–3153.
Shan, C., Yang, H., Han, D., Zhang, Q., Ivaska, A., Niu, L., 2010. Biosensors & Bioelectronics 25, 1070–1074.
Shan, C., Yang, H., Song, J., Han, D., Ivaska, A., Niu, L., 2009. Analytical Chemistry 81, 2378–2382.
Shao, Y., Wang, J., Engelhard, M., Wang, C., Lin, Y., 2009. Journal of Materials Chemistry 20, 743–748.
Tanne, C., G bel, G., Lisdat, F., 2010. Biosensors & Bioelectronics 26, 530–535.
Tasca, F., Gorton, L., Harreither, W., Haltrich, D., Ludwig, R., No ll, G., 2008. Journal of Physical Chemistry C 112, 9956–9961.
Tominaga, M., Nomura, S., Taniguchi, I., 2008. Electrochemistry Communications 10, 888–890.
Vaze, A., Hussain, N., Tang, C., Leech, D., Rusling, J., 2009. Electrochemistry Communications 11, 2004–2007.
Villar-Rodil, S., Paredes, J.I., Martínez-Alonso, A., Tascón, J.M.D., 2009. Journal of Materials Chemistry 19, 3591–3593.
Wang, D., Chen, L., 2009a. Electrochimica Acta 54, 4316–4320.
Wang, J., Li, M., Shi, Z., Li, N., Gu, Z., 2002. Analytical Chemistry 74, 1993–1997.
Wang, K., Liu, Q., Guan, Q.M., Wu, J., Li, H.N., Yan, J.J., 2011. Biosensors & Bioelectronics 26, 2252–2257.
Wang, Z., Liu, S., Wu, P., Cai, C., 2009b. Analytical Chemistry 81, 1638–1645.
Wang, Z., Zhou, X., Zhang, J., Boey, F., Zhang, H., 2009c. Journal of Physical Chemistry C 113, 14071–14075.
Wen, D., Liu, Y., Yang, G., Dong, S., 2007. Electrochimica Acta 52, 5312–5317.
Wu, H., Wang, J., Kang, X., Wang, C., Wang, D., Liu, J., Aksay, I.A., Lin, Y., 2009. Talanta 80, 403–406.
Xu, C., Wang, X., 2009. Small 5, 2212–2217.
Yang, W., Ratinac, K.R., Ringer, S.P., Thordarson, P., Gooding, J.J., Braet, F., 2010. Angewandte Chemie-International Edition 49, 2114–2138.
Yu, D., Yam, V.W.W., 2005. Journal of Physical Chemistry B 109, 5497–5503.
Yuan, J., Wang, K., Xia, X., 2005. Advanced Functional Materials 15, 803–809.
Zhao, H.Z., Sun, J.J., Song, J., Yang, Q.Z., 2010. Carbon 48, 1508–1514.
Zhao, M., Wu, X., Cai, C., 2009. Journal of Physical Chemistry C 113, 4987–4996.
Zhao, S., Zhang, K., Bai, Y., Yang, W., Sun, C., 2006. Bioelectrochemistry 69, 158–163.
Zhao, X., Mai, Z., Kang, X., Zou, X., 2008. Biosensors & Bioelectronics 23, 1032–1038.
Zhou, X., Huang, X., Qi, X., Wu, S., Xue, C., Boey, F.Y.C., Yan, Q., Chen, P., Zhang, H., 2009a. Journal of Physical Chemistry C 113, 10842–10846.
Zhou, Y., Bao, Q., Tang, L.A.L., Zhong, Y., Loh, K.P., 2009b. Chemistry of Materials 21, 2950–2956.
Zhou, Y., Yang, H., Chen, H.Y., 2008. Talanta 76, 419–423.
Zhu, L., Zhai, J., Guo, Y., Tian, C., Yang, R., 2006. Electroanalysis 18, 1842–1846.
Zou, Y., Xiang, C., Sun, L.X., Xu, F., 2008. Biosensors & Bioelectronics 23, 1010–1016.